Product Jahn-Teller systems: The $\{T_1 \otimes H\} \otimes (g+2h)$ icosahedral exciton

Q. C. Qiu
Department of Physics and Information, Medical College, Shantou University, Shantou 515031, People's Republic of China

L. F. Chibotaru and A. Ceulemans*
Department of Chemistry, Catholic University of Leuven, Celestijnenlaan 200F, B-3001 Leuven, Belgium
(Received 15 June 2001; published 13 December 2001)

The $\{T_1 \otimes H\} \otimes (g+2h)$ product Jahn-Teller (JT) system offers a model Hamiltonian for the excited configuration of C_{60}. It describes the combined JT activity of two open shells transforming as the threefold and fivefold degenerate icosahedral representations T_1 and H. The two separate JT problems interfere via the interaction with common vibrational modes. In this paper we examine the structure of the resulting potential energy surface. The treatment first considers the simplified $\{T_1 \otimes H\} \otimes (2h)$ problem. The coupling conditions for this problem can be represented in a two-dimensional phase diagram with a rich structure. The diagram is separated in four domains by four trough lines. These correspond to different embeddings of SO(3) in SO(5) and describe the possible spherical couplings between a three vector and a five tensor. Outside the trough lines symmetry is broken to D_{5d}, D_{3d}, D_{2h}, and even C_{2h}. Several tables offer a description of the structural aspects of these low-symmetry solutions. In the second part the full multimode Hamiltonian is treated by the method of the isostationary function. It is shown that the interconfigurational coupling term of this Hamiltonian reduces to the same tensorial form as for the simplified single mode $\{T_1 \otimes H\} \otimes (2h)$ case.

DOI: 10.1103/PhysRevB.65.035104 PACS number(s): 71.70.Ej, 73.61.Wp

I. INTRODUCTION

The excited and ionic states of C_{60} host many challenging Jahn-Teller (JT) problems.[1] In this paper we will be concerned with the lowest excited triplet and singlet states of neutral C_{60}, which both give rise to emission spectra with a rich vibronic structure.[2,3] These states have already been the subject of computational studies,[4–6] but a transparent model of the Jahn-Teller nature of the exciton is still lacking.

In the excited state two sources of JT activity exist: the fivefold degenerate hole state, created by removal of an electron from the filled H_u-HOMO, gives rise to a JT problem of type $H \otimes (g+2h)$, and the threefold degenerate electron state, formed by population of the empty T_{1u}-LUMO, exhibits a JT effect of type $T \otimes h$.

What is novel and interesting about the lowest excited states of the neutral buckminsterfullerene is that they combine two instabilities in a coupled or product Jahn-Teller problem of type $\{T_1 \otimes H\} \otimes (g+2h)$. In this paper we characterize the distortions in coordinate space which result from these combined instabilities. We examine the rotational symmetries which can arise when a three vector and a five tensor are combined, and construct a phase diagram of the possible coupling schemes. Actual calculations for the excited C_{60} will be reported in a subsequent work. Preliminary to the present problem we have reported the solution of the $\{T_1 \otimes T_2\} \otimes (e+t_2)$ product case.[7] This case is less intricate since it involves the coupling of two three vectors, and may serve as a useful starting point for the present analysis.

II. THE SINGLE MODE $\{T_1 \otimes H\} \otimes 2h$ HAMILTONIAN

At the start two important caveats must be brought under attention. First of all the treatment focuses on the "static" structure of the adiabatic potential energy surface of the coupled JT problem in the space of the active coordinates. This means that in the Hamiltonian the kinetic energy of the vibrating nuclei is not included. Once the nature of the surface has been determined it may be required to consider explicitly the role of the kinetic energy operator to study the quantum coherence effects, which are usually referred to as the "dynamic" aspects.

Secondly two-electron operators, describing the Coulombic and exchange interactions, are not included either. This is markedly different from standard Jahn-Teller treatments where the configurations are first separated into multiplets, which are then studied as isolated Jahn-Teller problems. As we have already mentioned in our first study of product systems,[7] our different approach is inspired by the special repulsion situation on the fullerene surface. Calculations suggest that several terms of the excited configuration in C_{60} are nearly degenerate.[5,6,8] Negri and Orlandi have performed simulations of the Jahn-Teller distorted emitting state, incorporating not less than three terms of the $h_u^9 t_{1u}^1$ configuration.[6] This exceptional repulsion situation has motivated us to switch to the product approach, which gives priority to the one-electron Hamiltonian and describes its full distortive power. In a later development these results must of course be combined with the two-electron part to study the influence of the Coulombic terms.

Only modes of h symmetry are able to correlate the H and T_1 parts of the product problem, since this is the only symmetry which is common to both H and T_1 instabilities. Hence the simplest Hamiltonian, which still describes the essential features of the problem, only considers a single h mode coupled both to H and T_1. We will mainly base our treatment on this Hamiltonian, in order to keep the formalism as transparent as possible. Extensions to the general case with multiple modes of both h and g symmetry are straightforward and will be presented in Sec. V. The single mode $\{T_1 \otimes H\} \otimes 2h$ Hamiltonian reads

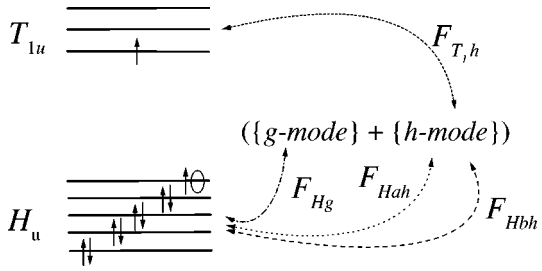

FIG. 1. Schematic description of the vibronic coupling of the product $\{T_1 \otimes H\} \otimes (g+2h)$ JT system. The two electronic levels are interacting via coupling to common vibrational modes.

$$\mathcal{H} = \sum_{\lambda \in h} (F_{Hah} \hat{L}^{Ha}_{h\lambda} + F_{Hbh} \hat{L}^{Hb}_{h\lambda} + F_{T_1h} \hat{L}^{T_1}_{h\lambda}) Q_{h\lambda} + \frac{1}{2} \sum_{\lambda \in h} K_h Q^2_{h\lambda}. \quad (1)$$

Here $\{Q_{h\lambda}\}$ spans the five components of the normal mode of h symmetry. The F symbols denote the linear JT force elements of the separate H and T_1 systems, while K_h is the elastic force constant of the h mode. Note that in our treatment F_{Hah} and F_{Hbh} are the force elements of the hole quintuplet. They are obtained from the orbital vibronic constants of the HOMO by simply inverting the signs. The single mode JT coupling scheme is illustrated in Fig. 1. The $\hat{L}$ quantities are operators, which are defined as

$$\hat{L}^{H\tau}_{h\lambda} = \sum_{\alpha,\beta \in H} \langle H\alpha | H\lambda H\beta \rangle_\tau c^+_\alpha c_\beta \quad (\tau = a,b), \quad (2)$$

$$\hat{L}^{T_1}_{h\lambda} = \sum_{i,j \in T_1} \langle T_1 i | H\lambda T_1 j \rangle c^+_i c_j. \quad (3)$$

The $\hat{L}^{H\tau}_{h\lambda}$ operator acts in the space of the five electronic components of H symmetry, via the creation and annihilation operators c^+_α and c_β. The $\langle H\alpha | H\lambda H\beta \rangle_\tau$ bracket denotes the complex conjugate of the appropriate Clebsch-Gordan coefficient. Note that there are two sets of independent $\langle H\alpha | H\lambda H\beta \rangle_\tau$ coupling coefficients, which are distinguished by the extra product multiplicity label $\tau = a,b$.

Similarly the $\hat{L}^{T_1}_{h\lambda}$ operator acts in the space of the T_1 triplet via the c^+_i and c_j operators. The corresponding $\langle T_1 i | H\lambda T_1 j \rangle$ coefficients are free of product multiplicities since the $T_1 \otimes T_1$ direct product is simply reducible. The $\hat{L}$ operators may be constructed from the standard product tables for the icosahedral group[9] and are listed for convenience in Appendix A. The respective electronic bases are expressed in real form as $|H\theta\rangle, |H\epsilon\rangle, |H\xi\rangle, |H\eta\rangle, |H\zeta\rangle$ and $|T_1x\rangle, |T_1y\rangle, |T_1z\rangle$, following the standard conventions of Boyle and Parker.[10]

III. THE ISOSTATIONARY FUNCTION

For a general description of the stationary points on the adiabatic surface we develop the isostationary function,[11,12] which expresses the extremal energies in terms of the eigenvector coefficients of the electronic state. To obtain this function we follow the procedure of Oepik and Pryce[13] and minimize the expectation value for the ground state energy in coordinate space, keeping the electronic variables fixed. The resulting extremal coordinates will be denoted as $\langle Q \rangle$, and the associated energy as $\langle ||E|| \rangle$. Both quantities are functions which are defined in the space of the electronic variables.

Since the Hamiltonian only contains one-particle operators, the electronic state can strictly be factorized as a product of a hole and an electron component, i.e.,

$$|\psi\rangle = (x|T_1x\rangle + y|T_1y\rangle + z|T_1z\rangle) \otimes (\theta|H\theta\rangle + \epsilon|H\epsilon\rangle + \xi|H\xi\rangle + \eta|H\eta\rangle + \zeta|H\zeta\rangle). \quad (4)$$

Hence only eight real eigenvector coefficients $x, y, \ldots, \zeta$, are needed to specify a state; they are subject to separate particle and hole normalization conditions

$$x^2 + y^2 + x^2 = 1, \quad \theta^2 + \epsilon^2 + \xi^2 + \eta^2 + \zeta^2 = 1. \quad (5)$$

Note that the five components of H transform as the orbital d-functions. According to the now standard Boyle and Parker convention the $|H\xi\rangle$, $|H\eta\rangle$, and $|H\zeta\rangle$ components transform as d_{yz}, d_{zx}, and d_{xy}, respectively, while the $|H\theta\rangle$ and $|H\epsilon\rangle$ transform as the linear combinations of d_{z^2} and $d_{x^2-y^2}$:

$$|H\theta\rangle = \sqrt{\frac{3}{8}} d_{3z^2-r^2} + \sqrt{\frac{5}{8}} d_{x^2-y^2},$$

$$|H\epsilon\rangle = \sqrt{\frac{3}{8}} d_{x^2-y^2} - \sqrt{\frac{5}{8}} d_{3z^2-r^2}.$$

In the setting of Boyle of Parker the cartesian coordinate frame has D_{2h} symmetry x,y,z transforming, respectively, as b_{3u}, b_{2u}, b_{1u}. Both d_{z^2} and $d_{x^2-y^2}$ are therefore of a_g symmetry, implying that they can be recombined in arbitrary ways. The isostationary function is given by

$$\langle ||E|| \rangle = \frac{5}{2} E^{JT}_{T_1h} \sum_\lambda (R^{T_1}_{h\lambda})^2 + \frac{5}{4} \sum_{\tau=a,b} E^{JT}_{H\tau h} \sum_\lambda (R^{H\tau}_{h\lambda})^2 + 2 \sum_\tau \frac{F_{T_1h} F_{H\tau h}}{K_h} \sum_\lambda (R^{T_1}_{h\lambda} R^{H\tau}_{h\lambda}). \quad (6)$$

Here the force elements and force constants are combined in effective JT energies, defined by

$$E^{JT}_{T_1h} = -\frac{1}{5} \frac{F^2_{T_1h}}{K_h}, \quad E^{JT}_{H\tau h} = -\frac{2}{5} \frac{F^2_{H\tau h}}{K_h}. \quad (7)$$

The R functions in the equation are obtained by taking the bracket of the $\hat{L}$ operators over ψ

$$R^{\Omega\tau}_{\Gamma\gamma} = \langle \psi | \hat{L}^{\Omega\tau}_{\Gamma\gamma} | \psi \rangle = \sum_{i,j} \langle \Omega\omega_j | \Gamma\gamma\Omega\omega_i \rangle_\tau x_i x_j, \quad (8)$$

with $x_i, x_j \in (x,y,z)$ for $\Gamma = T_1$, and $x_i, x_j \in (\theta, \epsilon, \xi, \eta, \zeta)$ for $\Gamma = H$. These functions are directly obtained from the 3Γ coupling tables, and are listed in Appendix B. The Appendix

also provides the expressions for the corresponding coordinates $\langle Q_{h\lambda}\rangle$ as a function of x_i and x_j. In deriving this expression the following orthogonality rule for R functions was used:

$$\sum_{\gamma} R^{Ha}_{\Gamma\gamma} R^{Hb}_{\Gamma\gamma} = 0 \quad \text{for} \quad a \neq b. \tag{9}$$

The isostationary function is a fourth rank tensor of the eigenvector coefficients. Its extremal points coincide with the extrema of the adiabatic JT surface. Although the isostationary function at first sight looks very complicated, it has in fact a nice transparent structure. The first term of $\langle||E||\rangle$ indeed coincides with the isostationary function of the $T_1 \otimes h$ system. As is well known, this function is a constant which corresponds to a Jahn-Teller trough of $T_1 \otimes h$ problem[1,14–17]

$$\frac{5}{2} E^{\mathrm{JT}}_{T_1 h} \sum_{\lambda} (R^{T_1}_{h\lambda})^2 = E^{\mathrm{JT}}_{T_1 h}. \tag{10}$$

Entirely similarly the second term corresponds to the isostationary function of the $H \otimes 2h$ problem[18]

$$\frac{5}{4} \sum_{\tau=a,b} E^{\mathrm{JT}}_{H\tau h} \sum_{\lambda} (R^{\tau H}_{h\lambda})^2 = \frac{1}{14}(5E^{\mathrm{JT}}_{hah} + 5E^{\mathrm{JT}}_{hbh}) + \frac{5}{56}(5E^{\mathrm{JT}}_{hah} - 9E^{\mathrm{JT}}_{hbh}) f, \tag{11}$$

with

$$f = \frac{7}{12}(\theta^2+\epsilon^2)^2 + \frac{7}{3}(\xi^2\eta^2 + \eta^2\zeta^2 + \zeta^2\xi^2) - \frac{7}{\sqrt{3}}\theta\epsilon(\xi^2-\eta^2) + \frac{7}{6}(\theta^2-\epsilon^2)(2\zeta^2-\xi^2-\eta^2) - \frac{1}{3}. \tag{12}$$

This function can be reduced to a constant trough potential under the equal coupling condition $5E^{\mathrm{JT}}_{Hah} = 9E^{\mathrm{JT}}_{Hbh}$, or in term of the force elements

$$\sqrt{5} F_{Hah} = \pm 3 F_{Hbh}. \tag{13}$$

In all other cases a warped potential is produced with either pentagonal (D_{5d}) or trigonal (D_{3d}) minima. Up to this point the product system is just the superposition of the JT effects of the hole and particle subsystems. The third term in $\langle||E||\rangle$, however, introduces new physics, since it gives rise to an interaction between the hole and particle via coupling to the same phonons. Both continuous and finite symmetries have to be involved to analyze the effect of this term, as will be demonstrated in the next section.

IV. EXTREMA OF THE ADIABATIC JT SURFACE

This section contains the core of our treatment. Using group-theoretical arguments we first derive coupling conditions which reduce the isostationary function to a constant equipotential trough. Two classes of solutions are found, depending on the relative signs of the $F_{H\tau h}$ and $F_{T_1 h}$ parameters. Subsequently we relax the strict trough conditions in order to obtain discrete minimal wells. The relative signs of the force elements continue to play an important role in this nondegenerate coupling regime: they discriminate between wells with high and low epikernel symmetries.

A. Trough conditions

To obtain an equipotential minimal energy trough, it is required that the system has rotational symmetry. In the case of a product system different rotational groups have to be combined. The $T_1 \otimes h$ part exhibits SO(3) symmetry, which can be identified as the free rotation of the T_1 electronic eigenvector in (x,y,z) space. There is a corresponding two-dimensional (2D) minimal energy trough in the space of the five h_g coordinates. On the other hand the full $H \otimes (g+2h)$ Hamiltonian attains SO(5) symmetry under suitable equal coupling conditions.[1,18,19] The H eigenvector then freely rotates in $(\theta,\epsilon,\xi,\eta,\zeta)$ space, while the system describes a 4D trough in the nine-dimensional $g_g + h_g$ coordinate space.

For the product system to have rotational symmetry, we thus must look for a suitable embedding of SO(3) in SO(5), i.e., an embedding which does not lift the degeneracy of the H manifold and furthermore yields a constant $T_1 \otimes H$ interaction term in the isostationary function. For this purpose we investigate first the branching rules of SO(5) representations upon symmetry reduction to SO(3).

In SO(5) the H manifold transforms as the fundamental vector representation (1,0). Its direct square reduces as follows:

$$(1,0)\otimes(1,0) = [(0,0)\oplus(2,0)]\oplus\{(1,1)\},$$

$$5\times 5 = [1+14]+\{10\},$$

where the second equation specifies the representational dimensions. The 14-dimensional (2,0) representation spans the $g+2h$ JT operators, listed in Appendix A. The so-called "physical" embedding of SO(3) in SO(5) yields the following branching scheme in the chain $SO(5)\downarrow SO(3)\downarrow I$:

$$(1,0)\rightarrow[2]\rightarrow H,$$

$$(2,0)\rightarrow\begin{cases}[2] & \rightarrow \quad h,\\ [4] & \rightarrow \quad g+h,\end{cases}$$

$$(1,1)\rightarrow\begin{cases}[1] & \rightarrow \quad T_1,\\ [3] & \rightarrow \quad T_2+G.\end{cases}$$

In this scheme the $[l]$ labels denote $(2l+1)$ degenerate irreducible representations of SO(3). It is clear that this embedding does not lift the degeneracy of the electronic space. The five components of H are indeed mapped on the five components of the quadrupolar tensor. On the other hand the JT modes are split into [2] and [4] symmetries, transforming in I as h and $g+h$, respectively. This offers a possibility to achieve equal coupling conditions for the product system. As we have argued before, the cross term between the T_1 and H instabilities can only involve modes of h symmetry. Hence as far as this cross term is concerned the g mode must be re-

moved from the JT space. The branching scheme shows that this can be done while keeping SO(3) invariance, simply by sacrificing the entire [4] part.

In summary an SO(3) product Hamiltonian requires that we apply the physical embedding and allow only interactions transforming as the [2] representation. The $H\otimes h[2]$ Hamiltonian can easily be constructed from the $(H\otimes h)_a$ and $(H\otimes h)_b$ subsystems by imposing the following constraint:

$$\sqrt{5}F_{Hah}=3F_{Hbh}. \tag{14}$$

This is indeed *one* of the coupling constraints which generate an isotropic $H\otimes h$ Hamiltonian. However, on inserting this condition in the isostationary function of the $H\otimes 2h$ problem we are confronted with a symmetry dilemma: according to the group theoretical argument we expect a solution with SO(3) symmetry, but the constant isostationary function implies that the energy is constant in a five-dimensional electronic space. The solution to this problem is that the group-theoretical treatment refers to the symmetry of the full $H\otimes h[2]$ Hamiltonian, while the isostationary function *only reflects the symmetry of the lowest sheet*. This is confirmed by the analysis of Chancey and O'Brien,[1] who demonstrate that the $H\otimes h[2]$ has two roots out of five (the lower and the upper ones) which form a four-dimensional hypersphere in the space of the h coordinates. The wave function of the ground state is based on a linear combination of the $Y^L_M(\theta,\varphi)$ spherical harmonics, with $L=2$, and the $D^L_{M\pm 2}(\gamma,\theta,\varphi)$ Wigner functions, with $L=2$, for the rigid rotator

$$|\psi\rangle=\sin(\alpha/2)|\psi_1(\gamma,\theta,\varphi)\rangle+\cos(\alpha/2)|\psi_2(\gamma,\theta,\varphi)\rangle, \tag{15}$$

where

$$|\psi_1\rangle=\begin{pmatrix} \frac{1}{2}\sqrt{\frac{3}{2}}\left[\cos^2\theta+\frac{1}{2}(-1+\sqrt{5}\cos 2\varphi)\sin^2\theta\right] \\ \frac{1}{8\sqrt{2}}[-(\sqrt{5}(1+3\cos 2\theta))+6\cos 2\varphi\sin^2\theta] \\ \frac{\sqrt{3}}{2}\sin 2\theta\sin\varphi \\ \frac{\sqrt{3}}{2}\sin 2\theta\cos\varphi \\ \frac{\sqrt{3}}{2}\sin 2\varphi\sin^2\theta \end{pmatrix} \tag{16}$$

and

$$|\psi_2\rangle=\begin{pmatrix} \frac{1}{8\sqrt{2}}\{-4\sqrt{5}\cos\theta\sin 2\gamma\sin 2\varphi+\cos 2\gamma[\sqrt{5}\cos 2\varphi(3+\cos 2\theta)+6\sin^2\theta]\} \\ \frac{1}{4}\sqrt{\frac{3}{2}}\{-2\cos\theta\sin 2\gamma\sin 2\varphi+\cos 2\gamma[\cos 2\varphi(1+\cos^2\theta)-\sqrt{5}\sin^2\theta]\} \\ -\cos\varphi\sin 2\gamma\sin\theta-\frac{1}{2}\cos 2\gamma\sin\varphi\sin 2\theta \\ \sin 2\gamma\sin\varphi\sin\theta-\frac{1}{2}\cos 2\gamma\cos\varphi\sin 2\theta \\ \cos 2\varphi\cos\theta\sin 2\gamma+\frac{1}{4}\cos 2\gamma(3+\cos 2\theta)\sin 2\varphi \end{pmatrix}. \tag{17}$$

We now insert these T_1 and H trough solutions in the third term of $\langle||E||\rangle$, which describes their interaction. Introducing $F_{Hh[2]}\equiv F_{Hbh}=(\sqrt{5}/3)F_{Hah}$ yields two trough solutions depending on the signs of the product $F_{Hh[2]}F_{T_1h}$. If $F_{Hh[2]}$ and F_{T_1h} have opposite sign we find a minimal energy trough which we will designate as the *normal trough*, in view of its correspondence with previously found solutions for the equal coupling regime for the $\{T_1\otimes T_2\}\otimes(e+t_2)$ problem.[7] It is characterized by $\alpha=\pi$, which implies that the H ground state reduces to the Y^2_M spherical harmonics and can be expressed as the tensor product of a T_1 vector with itself. The three components of this vector will be denoted as (a,b,c) to make clear distinction with the (x,y,z) components of the T_1 vector in the other shell. One then has from the $T_1\otimes T_1=H$ coupling table

$$\begin{aligned} \theta&=\frac{1}{2}\sqrt{\frac{3}{2}}(\phi^{-1}a^2-\phi b^2+c^2), \\ \epsilon&=\frac{1}{2}\sqrt{\frac{1}{2}}(\phi^2a^2-\phi^{-2}b^2-\sqrt{5}c^2), \\ \xi&=\sqrt{3}bc, \\ \eta&=\sqrt{3}ca, \end{aligned} \tag{18}$$

$$\zeta = \sqrt{3}ab,$$

where both (a,b,c) and $(\theta,\epsilon,\xi,\eta,\zeta)$ are normalized, and $\phi = \frac{1}{2}(1+\sqrt{5})$ is the golden mean. Substituting these expressions for the H vector in the isostationary function, yields

$$\langle||E||\rangle_{\omega} = E^{\mathrm{JT}}_{T_1 h} + E^{\mathrm{JT}}_{Hh[2]} - \frac{\sqrt{2}}{5}[1-3\cos^2\omega]\frac{F_{Hh[2]}F_{T_1 h}}{K_h}, \tag{19}$$

where ω denotes the angle between the (a,b,c) and (x,y,z) vectors

$$\cos\omega = ax + by + cz. \tag{20}$$

This function indeed represents a constant equipotential trough. Since $F_{Hh[2]}$ and $F_{T_1 h}$ were taken to have opposite signs, its energy is minimal for $\omega = 0$ or π:

$$\langle||E||\rangle_{\omega=0,\pi} = E^{\mathrm{JT}}_{T_1 h} + E^{\mathrm{JT}}_{Hh[2]} + \frac{2\sqrt{2}}{5}\frac{F_{Hh[2]}F_{T_1 h}}{K_h}$$

$$= -\frac{1}{5K_h}[F_{T_1 h} - \sqrt{2}F_{Hh[2]}]^2. \tag{21}$$

We thus retrieve a solution which is reminiscent of the spherical symmetry obtained by the concerted rotation of two three vectors in the $T_1 \otimes T_2$ problem.[7] In the present case the continuous symmetry combination of a three vector and a five vector is achieved by constructing the five vector as a tensor representation of another three vector, which then forms with the previous one a rotating pair. The angle between the two is zero (or π) meaning that these directions are parallel. For the $\{T_1 \otimes T_2\} \otimes (e + t_2)$ case this parallel solution was found for equal signs of the two JT force elements. In the present case the parallel solution is found for opposite signs. This difference is not essential though, since it only depends on the conventional choice of an external phase in the appropriate Clebsch-Gordan coefficients. The structural characteristics of the JT distortion in the normal trough will be further discussed in Sec. IV B.

Subsquently we have to consider the case where $F_{Hh[2]}$ and $F_{T_1 h}$ have the same sign. In analogy with the $T_1 \otimes T_2$ treatment one could have anticipated that this case simply corresponds to a ''perpendicular'' solution where H is based on a three vector (a,b,c) which is perpendicular to the (x,y,z) vector of T_1. However, this is not the lowest energy solution. The actual solution has a more intricate symmetry and corresponds to $\alpha = 0$. The H vector for this case consists of the rigid rotator function $D^2_{M\pm 2}(\theta,\varphi,\chi)$, as described in Eq. (17). As compared to the T_1 components defined in (θ,φ) space the five vector has an additional angular degree of freedom χ, which does not affect the coordinates and therefore is purely electronic. As a result under this coupling condition the ground state is twofold degenerate and will be decribed by the two rotator functions

$$|\psi\rangle = |\psi_2(\gamma,\theta,\varphi)\rangle, \quad |\psi'\rangle = |\psi_2(\gamma+\pi/4,\theta,\varphi)\rangle. \tag{22}$$

The energy of the trough is given by

$$\langle||E||\rangle = -\frac{1}{5K_h}(\sqrt{2}F_{Hh[2]} + F_{T_1 h})^2. \tag{23}$$

We have chosen to call this state an ''anti-Jahn-Teller trough,'' since it is degenerate and therefore violates the Jahn-Teller theorem. One should not forget though that the violation is only the result of a restrictive coupling condition and will disappear if further interactions are included. In the anti-Jahn-Teller trough the hole and electron parts of the system distort in opposite directions, such as to leave the H hole in a degenerate state. Chancey and O'Brien[1] have noticed before that the $H \otimes h[2]$ Hamiltonian sheets may meet in a certain domain of the SO(5) space. We now observe that precisely this domain is projected out in the anti-Jahn-Teller trough, and that it forms an SO(3) subspace of SO(5).

So far we have examined the ''physical'' embedding of SO(3) in SO(5) and shown that it successfully generates two typical equipotential minimal energy troughs. As we have indicated before [Eq. (14)] the $H \otimes h$ subsystem also can be made isotropic by applying the alternative coupling condition

$$-\sqrt{5}F_{Hah} = 3F_{Hbh}. \tag{24}$$

In this condition the sign of $\sqrt{5}$ has been changed as compared to the preceding one. In the character table of the icosahedral group such irrational conjugation interchanges T_1 and T_2 representations.[9] Judd and Lo[20] have invented the name ''kaleidoscope operator'' $\mathcal{K}$ to denote this interchange. The H representation is self conjugate. Under the action of $\mathcal{K}$ the $T_1 \otimes T_1 = H$ tensor product switches to a $T_2 \otimes T_2 = H$ tensor product, and the components of H change accordingly. As a result the conjugate coupling condition gives rise to an isotropic $H \otimes h[\overline{2}]$ Hamiltonian, where the $\overline{2}$ refers to a tensor product of T_2 vectors. The corresponding invariance group, say $\mathrm{SO}'(3)$, is a Weyl reflection of the physical SO(3) group in the root diagram of the SO(5) parent group.[21] This $H \otimes h[\overline{2}]$ Hamiltonian precisely corresponds to the one which was considered in the first study of icosahedral JT problems by Khlopin *et al.*[22] The troughlike solution, which these authors found, confirms its isotropic character. For the product problem the $\mathrm{SO}'(3)$ invariance is expected to be present in the $\{T_2 \otimes H\} \otimes h[\overline{2}]$ product, since this is the precise kaleidoscopic image of the $\{T_1 \otimes H\} \otimes h[2]$ case. This result is indeed easily verified analytically.

To our surprise the mixed product problems $\{T_1 \otimes H\} \otimes h[\overline{2}]$ or $\{T_2 \otimes H\} \otimes h[2]$ also exhibit spherical troughs in their ground states. This is again due to the fact that, while the full $H \otimes h[\overline{2}]$ Hamiltonian has only $\mathrm{SO}'(3)$ symmetry, its lowest root is in fact a four-dimensional trough with not less than SO(5) symmetry. Hence as far as the ground state is concerned, the symmetry of the mixed Hamiltonian of type $\{T_1 \otimes H\} \otimes h[\overline{2}]$ is described by

$$\mathrm{SO}'(3) \cap \mathrm{SO}(5) = \mathrm{SO}'(3). \tag{25}$$

We emphasize once more that this exceptionally high symmetry is only a property of the lowest and highest sheet of the $H \otimes h[\overline{2}]$ adiabatic energy surface, and is not retrieved

TABLE I. Trough conditions and energies for the $\{T_1\otimes H\}\otimes(2h)$ coupling.

Condition	$F_{Hh[2]}=F_{Hbh}=\frac{\sqrt{5}}{3}F_{Hah}$	$F_{Hh[\bar{2}]}=F_{Hbh}=-\frac{\sqrt{5}}{3}F_{Hah}$
$F_{Hbh}F_{T_1h}<0$	$-\frac{1}{5K_h}(\sqrt{2}F_{Hh[2]}-F_{T_1h})^2$	$-\frac{1}{5K_h}(\sqrt{2}F_{Hh[\bar{2}]}-F_{T_1h})^2$
	"normal" trough $\alpha=\pi,\omega=0,\pi$	SO′(3)
$F_{Hbh}F_{T_1h}>0$	$-\frac{1}{5K_h}(\sqrt{2}F_{Hh[2]}+F_{T_1h})^2$	$-\frac{1}{5K_h}(\sqrt{2}F_{Hh[\bar{2}]}+F_{T_1h})^2$
	"anti-JT" trough $\alpha=0$	SO′(3)

for the sheets in between. Moreover as shown by Manini and De Los Rios,[23] the low-lying states of the $H\otimes h[2]$ dynamic spectrum have SO(3) degeneracies only. Introducing $F_{Hh[\bar{2}]}=F_{Hbh}=-(\sqrt{5}/3)F_{Hah}$ into the isostationary function yields spherical symmetry troughs, for either sign of $F_{T_1h}F_{Hh[\bar{2}]}$. Energies are as in Eqs. (21) and (23) for negative and positive sign of $F_{T_1h}F_{Hh[\bar{2}]}$, respectively. Anti-Jahn-Teller behavior is not observed since the intersection of SO′(3) and SO(5) does not coincide with the $\alpha=0$ sphere.

As a result we find altogether four spherical troughs for the $\{T_1\otimes H\}\otimes(2h)$ product problem. They are summarized once more in Table I.

B. Phase diagram for the $T_1\otimes H$ exciton

As can be seen from Eq. (6) the actual ground state energy of the $T_1\otimes H$ problem only depends on three parameters $F_{Hah}, F_{Hbh}, F_{T_1h}$, and therefore can be represented in a two-dimensional diagram based on the parameter ratios F_{Hah}/F_{T_1h} and F_{Hbh}/F_{T_1h}. The results of an extensive analysis as a function of these parameters are presented in the phase diagram of Fig. 2. In the diagram one immediately

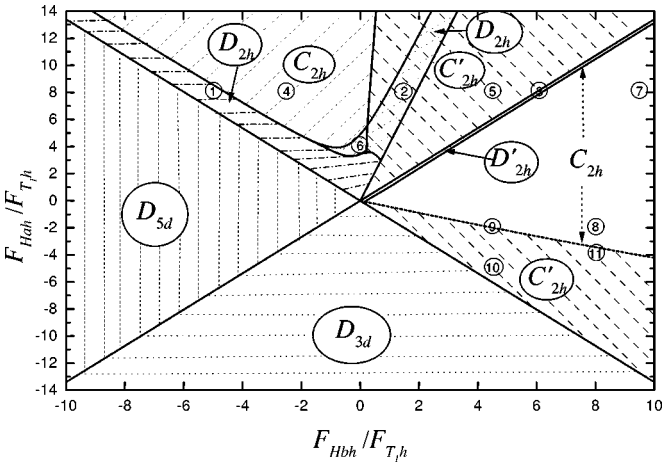

FIG. 2. Phase diagram for the $T_1\otimes H$ exciton. The encircled numbers refer to the stationary points described in Tables IV–VI. For the minima of D_{5d} and D_{3d} symmetry, the domains are clear. But for other symmetries in the system, detailed explanations are given in the text.

recognizes the straight lines through the origin which correspond to the SO(3) and SO′(3) troughs described previously. These lines divide the diagram in four "wedges," left and right, upper and lower. The straight line with positive slope is the $\{T_1\otimes H\}\otimes h[2]$ Hamiltonian with SO(3) symmetry. For negative ratios of $F_{Hh[2]}/F_{T_1h}$, i.e., left from the origin in Fig. 2, we find the normal trough. The JT surface consists of a 2D spherical trough in the 5D coordinate space. The curvature of the surface is expressed analytically by the following Hessian eigenvalues:

$$\left\{0,0,K_h,\frac{F_{T_1h}K_h}{-\sqrt{2}F_{Hh[2]}+F_{T_1h}},\frac{F_{T_1h}K_h}{-\sqrt{2}F_{Hh[2]}+F_{T_1h}}\right\}. \tag{26}$$

In Appendix C expressions are presented for the angular momentum operators in Q space. Exactly the same operators are found for the H part of the electronic space since both Q and H transform as a quadrupolar $[l=2]$ tensor. The T_1 part forms the basic $[l=1]$ vector of this space. As the diagram indicates this trough solution is found at the intersection of the regions of D_{3d} and D_{5d} symmetries, which are the highest epikernel symmetries of the problem. An entirely similar degenerate trough solution is found for instance in the cubic $T\otimes(e+t_2)$ problem on the line of coexistence of trigonal and tetragonal wells.[24,25] Across the origin the signs of the parameter ratios are switched and the trough adopts its anti-JT phase in which the H tensor is constructed from a rigid rotator function. High epikernel symmetries are banned from this trough and it is indeed surrounded by a region of low epikernel symmetries. Furthermore the Hessian eigenvalues in Q space are now given by

$$\left\{0,0,K_h,K_h,\frac{F_{T_1h}K_h}{\sqrt{2}F_{Hbh}+F_{T_1h}}\right\}. \tag{27}$$

The straight line with negative slope corresponds to the coupling condition for the $\{T_1\otimes H\}\otimes h[\bar{2}]$ Hamiltonian, which also has an isotropic adiabatic potential in the ground state. This line divides the diagram in a high and low symmetry domain. Below the line in the left and lower wedge one encounters the high epikernel phases, above it in the right and upper wedge only D_{2h} and C_{2h} are found.

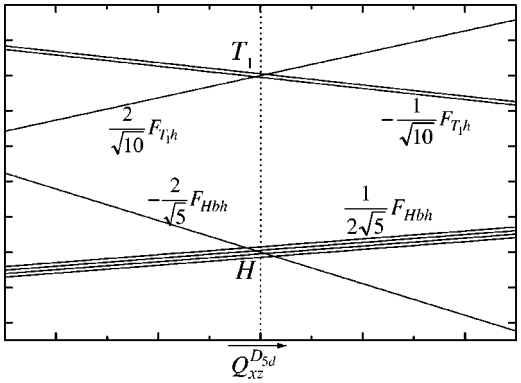

FIG. 3. Pentagonal distortion with the splitting of the parent terms along $Q_{xz}^{D_{5d}}$. The JT forces acting on the orbital singlet components of H and T_1 are given by $-(2/\sqrt{5})F_{Hbh}$ and $(2/\sqrt{10})F_{T_1}$ respectively.

If the equal coupling condition is relaxed, warping terms enter in the potential and will give rise to minimal energy wells and turning points. According to the epikernel principle[14] these points are expected to be characterized by epikernel symmetries, corresponding to intermediate groups in the tree structure of the parent I_h group $D_{5d}, D_{3d}, D_{2h}, C_{2h}$. In the isolated JT systems the highest epikernel symmetries D_{5d} and D_{3d}, prevail, but—as we have shown in the previous study of the $T_1 \otimes T_2$ problem[7]—in excitonic systems coupling conditions can be such that high epikernel symmetries are avoided and lower symmetry solutions will occur. This is not the case in the left and lower wedges surrounding the normal trough, where hole and electron act in parallel, as can indeed be seen in the phase diagram.

We will now discuss the various regions in order of decreasing symmetry. The highest epikernel is the D_{5d} point group. There are six equivalent pentagonal directions, one of which is described by

$$Q_{xz}^{D_{5d}} = \frac{1}{\sqrt{10}}(\sqrt{3}Q_\theta - Q_\epsilon + \sqrt{6}Q_\eta). \tag{28}$$

In Fig. 3, we present the splitting of the parent terms along $Q_{xz}^{D_{5d}}$. The JT forces acting on the orbital singlet components of H and T_1 are given by $-(2/\sqrt{5})F_{Hbh}$ and $+(2/\sqrt{10})F_{T_1h}$ respectively. We remind the reader that the splitting in this figure refers to term energies. In the case of excited C_{60} the H term represents a ${}^2H(h_u^9)$. The splitting of the corresponding h_u orbitals is of course the inverse of the splitting of this hole term. For a stable pentagonal minimum to develop F_{Hbh} and F_{T_1h} are thus required to have opposite signs so that both shells will distort in the same direction. Otherwise the pentagonal distortions will be unable to remove the remaining ground state degeneracy no matter in which direction they act, implying that further symmetry lowering distortions will occur. This is also reflected in the energy expression for the D_{5d} minimum

$$E_{D_{5d}} = -\frac{1}{5K_h}(\sqrt{2}F_{Hbh} - F_{T_1h})^2. \tag{29}$$

Clearly this expression will be minimal if F_{Hbh} and F_{T_1h} have different sign. F_{Hah} is not involved in the JT force along the pentagonal distortions. We thus find the region of existence of the pentagonal minima in the left wedge along the negative horizontal F_{Hbh}/F_{T_1} axis. The $F_{T_1h}F_{Hbh} < 0$ coupling regime ranges the pentagonal solutions in the $\omega = 0$ coupling class of the normal trough. The corresponding H eigenvector can indeed be written as tensor product of a three vector (a,b,c) which is exactly parallel to the (x,y,z) vector of the T_1 shell. The ground state eigenvectors and the corresponding distortion coordinates for the six pentagonal minima are listed in Table II. The extent of the $Q^{D_{5d}}$ distortion is expressed as

TABLE II. Electronic states and stationary coordinates for pentagonal minima with the ground energy of $E_{D_{5d}}$ and condition of $F_{T1}F_{Hbh} < 0$.

Label	$(a,b,c)\otimes(x,y,z)$	$\langle Q_\theta \rangle$	$\langle Q_\epsilon \rangle$	$\langle Q_\xi \rangle$	$\langle Q_\eta \rangle$	$\langle Q_\zeta \rangle$
P_1	$\frac{1}{\mu}(0,\phi,1)\otimes\frac{1}{\mu}(0,\phi,1)$	$-\sigma\sqrt{\frac{3}{10}}$	$-\sigma\sqrt{\frac{1}{10}}$	$\sigma\sqrt{\frac{3}{5}}$	0	0
P_2	$\frac{1}{\mu}(0,-\phi,1)\otimes\frac{1}{\mu}(0,-\phi,1)$	$-\sigma\sqrt{\frac{3}{10}}$	$-\sigma\sqrt{\frac{1}{10}}$	$-\sigma\sqrt{\frac{3}{5}}$	0	0
P_3	$\frac{1}{\mu}(1,0,\phi)\otimes\frac{1}{\mu}(1,0,\phi)$	$\sigma\sqrt{\frac{3}{10}}$	$-\sigma\sqrt{\frac{1}{10}}$	0	$\sigma\sqrt{\frac{3}{5}}$	0
P_4	$\frac{1}{\mu}(1,0,-\phi)\otimes\frac{1}{\mu}(1,0,-\phi)$	$\sigma\sqrt{\frac{3}{10}}$	$-\sigma\sqrt{\frac{1}{10}}$	0	$-\sigma\sqrt{\frac{3}{5}}$	0
P_5	$\frac{1}{\mu}(\phi,1,0)\otimes\frac{1}{\mu}(\phi,1,0)$	0	$\sigma\sqrt{\frac{2}{5}}$	0	0	$\sigma\sqrt{\frac{3}{5}}$
P_6	$\frac{1}{\mu}(-\phi,1,0)\otimes\frac{1}{\mu}(-\phi,1,0)$	0	$\sigma\sqrt{\frac{2}{5}}$	0	0	$-\sigma\sqrt{\frac{3}{5}}$

[a] $\phi = \frac{1}{2}(1+\sqrt{5})$, and $\mu = \sqrt{2+\phi}$ is the normalization factor.

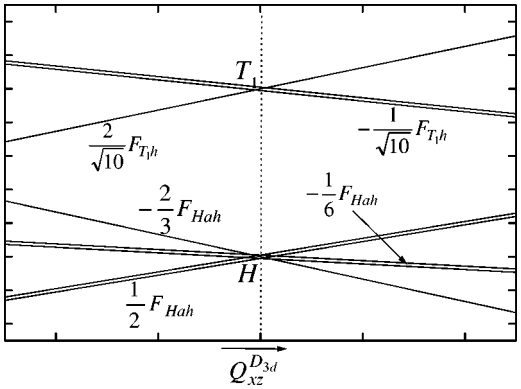

FIG. 4. Trigonal distortion with the splitting of the parent terms along $Q_{xz}^{D_{3d}}$. The JT forces acting on the orbital singlet components of H and T_1 are given by $-\frac{2}{3}F_{Hah}$ and $(2/\sqrt{10})F_{T_1}$, respectively.

$$\sigma=\langle Q_{xz}^{D_{5d}}\rangle=\frac{\sqrt{2}}{\sqrt{5}K_h}(\sqrt{2}F_{Hbh}-F_{T_1h}). \tag{30}$$

Entirely similar considerations apply to the alternative high symmetry epikernel D_{3d}, where F_{Hah} takes over the role of F_{Hbh}. A trigonal distortion coordinate is given by

$$Q_{xz}^{D_{3d}}=\frac{1}{\sqrt{6}}(Q_\theta+\sqrt{3}Q_\epsilon+\sqrt{2}Q_\eta). \tag{31}$$

Figure 4 shows the splitting pattern. The orbital singlets are subject to forces $(2/\sqrt{10})F_{T_1h}$ and $-\frac{2}{3}F_{Hah}$ for T_1 and H respectively. Hence trigonal minima are coupled when F_{Hah} is dominant over F_{Hbh} and $F_{T_1h}F_{Hah}<0$. This puts the trigonal phase in the lower wedge along the negative vertical axis in the phase diagram. Again these points are elements of the normal trough. In Table III we list the eigenvectors and distortion coordinates for the ten equivalent trigonal minima. The corresponding energy and extent of distortion are given by

$$E_{D_{3d}}=-\frac{1}{45K_h}(\sqrt{10}F_{Hah}-3F_{T_1h})^2=-\frac{1}{2}K_h\rho^2,$$

$$\rho=\langle Q_{xz}^{D_{3d}}\rangle=\frac{\sqrt{2}}{3\sqrt{5}K_h}(\sqrt{10}F_{Hah}-3F_{T_1h}).$$

Next we consider the lower epikernel symmetry D_{2h}. The orthorhombic group completely resolves the electronic manifolds $T_1\rightarrow B_1+B_2+B_3$, $H\rightarrow 2A+B_1+B_2+B_3$. As a result different kinds of exciton states can be formed. There are essentially three distinct configurations, which can be denoted as B_1A, B_1B_1, B_1B_2 exemplified by the nonzero eigenvector composition $(z)(\theta,\epsilon),(z)(\zeta),(z)(\eta)$, respectively. The corresponding energies are given by

TABLE III. Electronic states and stationary coordinates for trigonal minima with the ground energy of $E_{D_{3d}}$ and condition of $F_{T1}F_{Hah}<0$.

Label	$(a,b,c)\otimes(x,y,z)$	$\langle Q_\theta\rangle$	$\langle Q_\epsilon\rangle$	$\langle Q_\xi\rangle$	$\langle Q_\eta\rangle$	$\langle Q_\zeta\rangle$
t_1	$\frac{1}{\sqrt{3}}(0,\phi^{-1},\phi)\otimes\frac{1}{\sqrt{3}}(0,\phi^{-1},\phi)$	$\rho/\sqrt{6}$	$-\sqrt{\frac{1}{2}}\rho$	$\rho/\sqrt{3}$	0	0
t_2	$\frac{1}{\sqrt{3}}(0,-\phi^{-1},\phi)\otimes\frac{1}{\sqrt{3}}(0,-\phi^{-1},\phi)$	$\rho/\sqrt{6}$	$-\sqrt{\frac{1}{2}}\rho$	$-\rho/\sqrt{3}$	0	0
t_3	$\frac{1}{\sqrt{3}}(\phi,0,\phi^{-1})\otimes\frac{1}{\sqrt{3}}(\phi,0,\phi^{-1})$	$\rho/\sqrt{6}$	$\sqrt{\frac{1}{2}}\rho$	0	$\rho/\sqrt{3}$	0
t_4	$\frac{1}{\sqrt{3}}(\phi,0,\phi^{-1})\otimes\frac{1}{\sqrt{3}}(\phi,0,\phi^{-1})$	$\rho/\sqrt{6}$	$\sqrt{\frac{1}{2}}\rho$	0	$-\rho/\sqrt{3}$	0
t_5	$\frac{1}{\sqrt{3}}(\phi^{-1},\phi,0)\otimes\frac{1}{\sqrt{3}}(\phi^{-1},\phi,0)$	$-\sqrt{\frac{2}{3}}\rho$	0	0	0	$\rho/\sqrt{3}$
t_6	$\frac{1}{\sqrt{3}}(-\phi^{-1},\phi,0)\otimes\frac{1}{\sqrt{3}}(-\phi^{-1},\phi,0)$	$-\sqrt{\frac{2}{3}}\rho$	0	0	0	$-\rho/\sqrt{3}$
t_7	$\frac{1}{\sqrt{3}}(1,1,1)\otimes\frac{1}{\sqrt{3}}(1,1,1)$	0	0	$\rho/\sqrt{3}$	$\rho/\sqrt{3}$	$\rho/\sqrt{3}$
t_8	$\frac{1}{\sqrt{3}}(-1,1,1)\otimes\frac{1}{\sqrt{3}}(-1,1,1)$	0	0	$\rho/\sqrt{3}$	$-\rho/\sqrt{3}$	$-\rho/\sqrt{3}$
t_9	$\frac{1}{\sqrt{3}}(1,-1,1)\otimes\frac{1}{\sqrt{3}}(1,-1,1)$	0	0	$-\rho/\sqrt{3}$	$\rho/\sqrt{3}$	$-\rho/\sqrt{3}$
t_{10}	$\frac{1}{\sqrt{3}}(1,1,-1)\otimes\frac{1}{\sqrt{3}}(1,1,-1)$	0	0	$-\rho/\sqrt{3}$	$-\rho/\sqrt{3}$	$\rho/\sqrt{3}$

TABLE IV. D_{2h} minima and their corresponding C_{2h} extrema in the upper and right wedges of the phase diagram (Calculations refer to points 1, 2, and 3 in Fig. 2).

Test points	$1^{B_1A}_{D_{2h}}$	$1^{BA}_{C_{2h}}$	$2^{B_1A}_{D_{2h}}$	$2^{BA}_{C_{2h}}$	$3^{B_1B_1}_{D_{2h}}$	$3^{BA}_{C_{2h}}$
F_{Hah}[a]	8	8	8	8	8	8
F_{Hbh}[a]	−5	−5	1.5	1.5	6.1	6.1
F_{T_1h}[a]	1	1	1	1	1	1
$\langle Q_\theta \rangle$	−3.577	−4.537	−3.405	−4.299	−3.653	3.179
$\langle Q_\epsilon \rangle$	4.617	−2.759	4.396	−1.527	4.813	−0.488
$\langle Q_\xi \rangle$	0	0	0	0	0	0
$\langle Q_\eta \rangle$	0	0	0	0	0	0
$\langle Q_\zeta \rangle$	0	−2.244	0	−3.453	0	5.108
Hessian Evals(1)[b]	1	1	1	1	1	1
Hessian Evals(2)	0.888	0.577	0.840	0.847	1.000	0.697
Hessian Evals(3)	0.211	0.248	0.114	0.689	0.033	0.015
Hessian Evals(4)	0.108	0.056	0.063	0.274	0.025	0.038
Hessian Evals(5)	0.031	−0.100	0.023	0.037	0.025	−0.015
Energy	−17.056	−16.615	−15.457	−16.366	−18.257	−18.220

[a] $K_h = 1$.

[b] Hessian eigenvalues are listed by the order of their absolute values.

$$E^{B_1A}_{D_{2h}} = -\frac{1}{80K_h}\left(\sqrt{5(3F^2_{Hah}+F^2_{Hbh})}+4|F_{T_1h}|\right)^2,$$

$$E^{B_1B_1}_{D_{2h}} = -\frac{1}{40K_h}\left[\frac{1}{3}\left(\sqrt{10}F_{Hah}+3F_{T_1h}\right)^2 + 5\left(\sqrt{2}F_{Hbh}+F_{T_1h}\right)^2\right], \tag{32}$$

$$E^{B_1B_2}_{D_{2h}} = -\frac{F^2_{T_1h}}{5K_h} - \frac{1}{12K_h}\left(F^2_{Hah}+3F^2_{Hbh}\right) - \frac{F_{T_1h}}{2\sqrt{10}K_h}\left(\phi^{-2}F_{Hbh}-\phi F_{Hah}\right).$$

Both AB_1 and B_1B_1 states can be minimal energy solutions but B_1B_2 is always a saddle point. In the diagram orthorhombic solutions are found both in upper and right wedges. Sample calculations for points marked 1, 2, and 3 in the diagram are reported in Table IV. In the upper wedge minimum energy D_{2h} solutions are of B_1A type. Point 1 belongs to a narrow region close to the SO′(3) trough where the surface has absolute minima of D_{2h} symmetry. Point 2 belongs to an adjacent domain where D_{2h} is coexistent with an absolute minimum of lower C_{2h} symmetry. In the right wedge there is a very narrow region bordering the anti-JT trough where an orthorhombic absolute minimum of type B_1B_1 exists. This region is indicated as D'_{2h} in the diagram and contains point 3.

In the other parts of the upper and right wedges we only find C_{2h} solutions. In this symmetry the electronic manifolds split as $T_1 \rightarrow A+2B$, $H \rightarrow 3A+2B$. There are therefore four possible ground state configurations which we will denote as AA, AB, BA, and BB, characterized by nonzero eigenvector compositions $(z)(\theta,\epsilon,\zeta)$, $(z)(\xi,\eta)$, $(x,y)(\theta,\epsilon,\zeta)$, $(x,y)(\xi,\eta)$, respectively. Here the C_2 axis was put along the Cartesian z direction. The only C_{2h} ground states that are encountered in the diagram are of AA and BA types. Of these the AA case can be described by the roots of an effective quartic equation while the other BA type is even more complicated. We thus have to recur to numerical diagonalization and minimization procedures to analyze the C_{2h} ground states. The C_{2h} solutions in the upper wedge are included in Table V. The domain characterized by point 4 has an absolute C_{2h} minimum of type AA. In the lower part of this domain is a small tip marked by point 6, where the absolute C^{AA}_{2h} minimum coexists with a secondary minimum of type $D^{B_1A}_{2h}$ as indicated in the diagram. In the domain marked by point 5 absolute C_{2h} minima are encountered of symmetry type BA and at this point the D_{2h} solution clearly has become a saddle point. As we have already discussed this domain contains a region, exemplified by point 2, where secondary $D^{B_1A}_{2h}$ minima coexist.

Finally the right wedge entirely consists of C_{2h} absolute minima, except for the narrow D'_{2h} region bordering the anti-JT trough. In the upper half of the wedge (points 7 and 8) one has C^{AA}_{2h} minima, as listed in Table VI. In this region the $D^{B_1B_1}_{2h}$ solutions form saddle points as we have indicated in the table for point 7. In the lower part of the wedge (points 10 and 11) the symmetry type of the C_{2h} ground state has changed to BA. The phase transition marking this switch of ground state is indicated by the dashed line in the diagram. Close to this line one of the Hessian eigenvalues becomes very small, as shown for point 8, 9, and 11. The calculations show that near this line C^{AA}_{2h} and C^{BA}_{2h} ground states are coexisting, as shown for point 9 in Table VI.

TABLE V. Examples of C_{2h} minima and D_{2h} extrema in the upper wedge of the phase diagram.

Example points	$4^{AA}_{C_{2h}}$	$4^{B_1A}_{D_{2h}}$	$5^{BA}_{C_{2h}}$	$5^{B_1A}_{D_{2h}}$	$6^{AA}_{C_{2h}}$	$6^{B_1A}_{D_{2h}}$
F_{Hah}[a]	8	8	8	8	4	4
F_{Hbh}[a]	−2.5	−2.5	4.5	4.5	0	0
F_{T_1h}[a]	1	1	1	1	1	1
$\langle Q_\theta \rangle$	−4.580	−3.436	−3.117	−3.542	−2.448	−1.887
$\langle Q_\epsilon \rangle$	1.665	4.436	−3.608	4.572	1.384	2.436
$\langle Q_\xi \rangle$	0	0	0	0	0	0
$\langle Q_\eta \rangle$	0	0	0	0	0	0
$\langle Q_\zeta \rangle$	2.998	0	−3.320	0	−1.301	0
Hessian Evals(1)[b]	1	1	1	1	1	1
Hessian Evals(2)	0.729	0.673	0.910	0.615	0.767	0.793
Hessian Evals(3)	0.610	0.543	0.225	0.370	0.699	0.205
Hessian Evals(4)	0.218	0.113	0.109	0.109	0.198	0.144
Hessian Evals(5)	0.098	−0.105	0.061	−0.042	0.041	0.038
Energy	−16.366	−15.739	−16.876	−16.723	−4.799	−4.749

[a] $K_h = 1$.
[b] Hessian eigenvalues are listed by the order of their absolute values.

V. THE GENERAL $\{T_1 \otimes H\} \otimes (g + 2h)$ HAMILTONIAN IN A MULTIMODE ENVIRONMENT

We now turn to the more general form of the Hamiltonian, which should be directly applicable to the excited states of C_{60}. As compared to the formalism in Sec. II normal modes are now denoted as $Q_{\mu\Gamma\gamma}$ where μ is an extra label which enumerates the modes of symmetry type Γ. The linear JT force elements receive a more general labeling as $F^{\Omega\tau}_{\mu\Gamma}$. Again here $\mu\Gamma$ is a particular mode, Ω denotes the symmetry of the electronic level ($\Omega = T_1, H$) and τ is the multiplicity index in the case of $H \otimes h$ coupling ($\tau = a, b$). The general form of the Hamiltonian is given by

$$H = \frac{1}{2} \sum_{\mu\Gamma\gamma} K_{\mu\Gamma} Q^2_{\mu\Gamma\gamma} + \sum_{\mu\Gamma\gamma} \left(\sum_{\tau} F^{H\tau}_{\mu\Gamma} \hat{L}^{H\tau}_{\Gamma\gamma} + F^{T_1}_{\mu\Gamma} \hat{L}^{T_1}_{\Gamma\gamma} \right). \tag{33}$$

The $\hat{L}$ operators are straightforward generalizations of the cases considered proviously, i.e.,

TABLE VI. Examples of C_{2h} minima in the right wedge of the phase diagram.

Label	$7^{AA}_{C_{2h}}$	$7^{B_1B_1}_{D_{2h}}$	$8^{AA}_{C_{2h}}$	$9^{BA}_{C_{2h}}$	$9^{AA}_{C_{2h}}$	$10^{BA}_{C_{2h}}$	$11^{BA}_{C_{2h}}$	$11^{AA}_{C_{2h}}$
F_{Hah}[a]	8	8	−2	−2	−2	−5	−4	−4
F_{Hbh}[a]	9.5	9.5	8	4.5	4.5	4.5	8	8
F_{T_1h}[a]	1	1	1	1	1	1	1	1
$\langle Q_\theta \rangle$	−0.927	−3.653	−0.394	0.387	−0.387	0.492	0.387	−0.388
$\langle Q_\epsilon \rangle$	6.255	7.218	5.033	2.446	3.046	2.029	4.425	5.026
$\langle Q_\xi \rangle$	0	0	0	0	0	0	0	
$\langle Q_\eta \rangle$	0	0	0	0	0	0	0	
$\langle Q_\zeta \rangle$	6.197	0	5.536	3.608	3.118	3.874	6.033	−5.542
Hessian Evals(1)[b]	1	1	1	1	1	1	1	1
Hessian Evals(2)	0.911	1	0.979	1	1	0.540	0.998	0.998
Hessian Evals(3)	0.782	0.453	0.783	0.684	0.684	0.273	0.645	0.645
Hessian Evals(4)	0.413	0.444	0.716	0.563	0.563	0.107	0.571	0.571
Hessian Evals(5)	4.1×10^{-4}	−1.236	4.6×10^{-6}	4.7×10^{-8}	1.7×10^{-8}	0.031	1.7×10^{-7}	-4.6×10^{-7}
Energy	−39.196	−32.720	−28.066	−9.573	−9.573	−9.682	−28.063[c]	−28.063[d]

[a] $K_h = 1$.
[b] Hessian eigenvalues are listed by the order of their absolute values.
[c] The accurate numerical result for this energy is −28.063000488.
[d] The accurate numerical result for this energy is −28.063000426.

$$\hat{L}^{H\tau}_{\Gamma\gamma}=\sum_{\alpha,\beta,\in H}\langle H\alpha|\Gamma\gamma H\beta\rangle_{\tau}c^{+}_{\alpha}c_{\beta},\quad(\tau=a,b),\tag{34}$$

$$\hat{L}^{T_1}_{\Gamma\gamma}=\sum_{i,j\in T_1}\langle T_1 i|\Gamma\gamma T_1 j\rangle c^{+}_{i}c_{j}.\tag{35}$$

The coupling coefficients in $\hat{L}^{H\tau}_{\Gamma\gamma}$ are defined for Γ's which are contained in the symmetrized square of $H\otimes H$, i.e., $\Gamma=A+G+2H$. For the $\hat{L}^{T_1}_{\Gamma\gamma}$ operator possible symmetries of active modes are limited to $[T_1\otimes T_1]$, i.e., $\Gamma=A+H$. No product multiplicities occur here and no extra τ label is therefore needed. The isostationary function for the electronic states $|\Psi\rangle$ described by the eigenvector coefficients (x,y,z) and $(\theta,\epsilon,\xi,\eta,\zeta)$ in the complete multimode Hamiltonian reads

$$\begin{aligned}\langle||E||\rangle=-\frac{1}{2}\sum_{\Gamma}\Bigg\{&S_{\Gamma}(T_1,T_1)\sum_{\gamma}(R^{T_1}_{\Gamma\gamma})^2\\&+\sum_{\tau}S_{\Gamma}(H\tau,H\tau)\sum_{\gamma}(R^{H\tau}_{\Gamma\gamma})^2\\&+2\sum_{\tau}S_{\Gamma}(T_1,H\tau)\sum_{\gamma}R^{T_1}_{\Gamma\gamma}R^{H\tau}_{\Gamma\gamma}\Bigg\}.\end{aligned}\tag{36}$$

The S parameters in this expression are effective coupling constants, which depend on the JT force elements and force constants

$$S_{\Gamma}(\Lambda\tau,\Lambda'\tau')=\sum_{\mu}\frac{F^{\Lambda\tau}_{\mu\Gamma}F^{\Lambda'\tau'}_{\mu\Gamma}}{K_{\mu\Gamma}}.\tag{37}$$

The R functions are the appropriate tensor expressions defined previously and listed in Appendix B. The totally symmetric R functions reduce to scalars in view of the normalization condition

$$\begin{aligned}R^{T_1}_{A}&=\frac{1}{\sqrt{3}}(x^2+y^2+z^2)=\frac{1}{\sqrt{3}},\\R^{H}_{A}&=\frac{1}{\sqrt{5}}(\theta^2+\epsilon^2+\xi^2+\eta^2+\zeta^2)=\frac{1}{\sqrt{5}}.\end{aligned}\tag{38}$$

As a result totally symmetric vibrations only produce global vertical shifts of the entire JT surface, and therefore will be left out from further consideration. The summation index Γ is thus restricted to $\Gamma=H$ for the T_1 contributions, and to $\Gamma=G,H$ for the H contributions. Although the generalized isostationary function at first sight looks very complicated, it is in fact a transparent expression. The first term in $S_{\Gamma}(T_1,T_1)$ indeed coincides with the isostationary function of the multimode T_1 subsystem. As is well known, this function is a constant and corresponds to the Jahn-Teller trough energy of the $T_1\otimes h$ problem:

$$-\frac{1}{2}S_H(T_1,T_1)\sum_{\gamma}(R^{T_1}_{\Gamma\gamma})^2=-\frac{1}{5}\sum_{\mu}\frac{(F^{T_1}_{\mu H})^2}{K_{\mu H}}=E^{\mathrm{JT}}_{T_1}.\tag{39}$$

In a similar way, the second term in $S_{\Gamma}(H\tau,H\tau)$ is the isostationary function of the $H\otimes(g+2h)$ subsystem. It can be expressed as

$$\begin{aligned}-\frac{1}{2}\sum_{\Gamma=G,H}\sum_{\tau}S_{\Gamma}(H\tau,H\tau)\sum_{\gamma}(R^{H\tau}_{\Gamma\gamma})^2&=\frac{1}{14}(4E^{\mathrm{JT}}_{G}+5E^{\mathrm{JT}}_{Ha}+5E^{\mathrm{JT}}_{Hb})\\&+\frac{5}{56}(4E^{\mathrm{JT}}_{G}+5E^{\mathrm{JT}}_{Ha}-9E^{\mathrm{JT}}_{Hb})f.\end{aligned}\tag{40}$$

The JT energies for the multimode case are given by

$$\begin{aligned}E^{\mathrm{JT}}_{G}&=-\frac{1}{2}\sum_{\mu}\frac{(F^{H}_{\mu G})^2}{K_{\mu G}},\\E^{\mathrm{JT}}_{Ha}&=-\frac{2}{5}\sum_{\mu}\frac{(F^{Ha}_{\mu H})^2}{K_{\mu H}},\\E^{\mathrm{JT}}_{Hb}&=-\frac{2}{5}\sum_{\mu}\frac{(F^{Hb}_{\mu H})^2}{K_{\mu H}}.\end{aligned}\tag{41}$$

The dependence on the eigenvector coefficients is contained in the function f, which is given in Eq. (12). Note that the multimode aspect of this JT problem is fully incorporated into the effective coupling constants, so that its isostationary function takes the same form as the single mode $H\otimes(g+2h)$ problem. As has been described in previous work this problem can be reduced to a trough potential under equal coupling conditions, which eliminate the factor in front of f, but in all other cases a warped potential will be produced with either pentagonal (D_{5d}) or trigonal (D_{3d}) minima. Up to this point the product system is just the superposition of the JT effects of the hole and particle subsystems. The third term in $S_{\Gamma}(T_1,H\tau)$ gives rise to an interaction between the hole and particle via coupling to the same phonons. One has

$$\begin{aligned}-\sum_{\Gamma}\sum_{\tau}S_{\Gamma}(T_1,H\tau)\sum_{\gamma}R^{T_1}_{\Gamma\gamma}R^{H\tau}_{\Gamma\gamma}&=-\sum_{\tau}\left(\sum_{\mu}\frac{F^{T_1}_{\mu H}F^{H\tau}_{\mu H}}{K_{\mu H}}\right)\sum_{\gamma}(R^{T_1}_{H\gamma}R^{H\tau}_{H\gamma}).\end{aligned}\tag{42}$$

As this expression shows the coupling can only arise through a common mode of H symmetry, since this is the only coordinate symmetry which is contained in both component problems. Moreover in spite of the multimode character all force constants are absorbed in only two parameters $S_H(T_1,Ha)$ and $S_H(T_1,Hb)$. The tensorial part of the interaction term is thus entirely the same as for the simple Hamiltonian considered in the previous section, the two effective S parameters playing the roles of F_{Hah} and F_{Hbh}. The phase diagram thus continues to offer a relevant classification, except that now superimposed on the distortions of H symmetry, there may be a further distortion in the coordinate space of G symmetry. It should also be kept in mind that in the multimode environment the curvature of the potential energy surface in the extremal points is described by a Hessian over all coordinates, which of course no longer coincides with the simple curvature expressions for the single mode case.

VI. CONCLUSION

In this paper we have made a start with the detailed examination of the $T_1 \otimes H$ exciton that governs the excited states of C_{60}. In the product system, the T_1 and H components interact with each other via modes of h symmetry. Our analysis was based on the continuous invariance group in this coordinate space. Quite remarkably, while the $H \otimes h$ Hamiltonian can only attain SO(3) symmetry as a whole, its ground state can under equal coupling condition reach full SO(5) symmetry. The study of the coupling term in this space is—in mathematical terms—equivalent to finding embeddings of SO(3) in SO(5). Four different solutions were obtained, corresponding to the four diagonal lines radiating from the center in Fig. 2, and summarized in Table I. For the normal and anti-JT troughs, explicit substitution formulas were presented which demonstrate the invariance of the isostationary function. Outside of the trough lines the diagram is clearly divided in a high and low epikernel region. These two regions were encountered in the preliminary study of the $T_1 \otimes T_2$ system, and depend on whether the two components of the exciton exert distortion forces in the same or in opposite directions. However, we have demonstrated that the combination of a three vector and five vector with opposing JT tendencies has a much richer tensorial structure than in the case of two three vectors. In subsequent work we will now concentrate on the analysis of the particular coupling conditions in actual C_{60}, in order to establish to what region of the diagram they belong.

ACKNOWLEDGMENTS

This research was supported by the Belgian National Science Foundation and the Belgian Goverment under the concerted action scheme.

APPENDIX A: $\hat{L}$ OPERATORS

$$\hat{L}^{T_1}_{h\theta}=\frac{1}{2}\sqrt{\frac{3}{5}}(\phi^{-1}c_1^+c_1-\phi c_2^+c_2+c_3^+c_3),$$

$$\hat{L}^{T_1}_{h\epsilon}=\frac{1}{2\sqrt{5}}(\phi^{2}c_1^+c_1-\phi^{-2}c_2^+c_2-\sqrt{5}c_3^+c_3),$$

$$\hat{L}^{T_1}_{h\xi}=\sqrt{\frac{3}{10}}(c_2^+c_3+c_3^+c_2),$$

$$\hat{L}^{T_1}_{h\eta}=\sqrt{\frac{3}{10}}(c_3^+c_1+c_1^+c_3),$$

$$\hat{L}^{T_1}_{h\zeta}=\sqrt{\frac{3}{10}}(c_1^+c_2+c_2^+c_1),$$

$$\hat{L}^{Ha}_{h\theta}=\frac{1}{2\sqrt{6}}(3c_\theta^+c_\theta-3c_\epsilon^+c_\epsilon-c_\xi^+c_\xi-c_\eta^+c_\eta+2c_\zeta^+c_\zeta),$$

$$\hat{L}^{Ha}_{h\epsilon}=-\frac{1}{2\sqrt{2}}[\sqrt{3}(c_\epsilon^+c_\theta+c_\theta^+c_\epsilon)-c_\xi^+c_\xi+c_\eta^+c_\eta],$$

$$\hat{L}^{Ha}_{h\xi}=-\frac{1}{12}[\sqrt{6}(c_\xi^+c_\theta+c_\theta^+c_\xi)-3\sqrt{2}(c_\xi^+c_\epsilon+c_\epsilon^+c_\xi)+4\sqrt{3}(c_\zeta^+c_\eta+c_\eta^+c_\zeta)],$$

$$\hat{L}^{Ha}_{h\eta}=\frac{1}{12}[\sqrt{6}(c_\eta^+c_\theta+c_\theta^+c_\eta)+3\sqrt{2}(c_\eta^+c_\epsilon+c_\epsilon^+c_\eta)+4\sqrt{3}(c_\zeta^+c_\xi+c_\xi^+c_\zeta)],$$

$$\hat{L}^{Ha}_{h\zeta}=\frac{1}{2\sqrt{3}}[\sqrt{5}(c_\zeta^+c_\theta+c_\theta^+c_\zeta)-2(c_\eta^+c_\xi+c_\xi^+c_\eta)],$$

$$\hat{L}^{Hb}_{h\theta}=\frac{1}{2\sqrt{2}}[c_\epsilon^+c_\theta+c_\theta^+c_\epsilon+\sqrt{3}(c_\xi^+c_\xi-c_\eta^+c_\eta)],$$

$$\hat{L}^{Hb}_{h\epsilon}=\frac{1}{2\sqrt{2}}(c_\theta^+c_\theta-c_\epsilon^+c_\epsilon+c_\xi^+c_\xi+c_\eta^+c_\eta-2c_\zeta^+c_\zeta),$$

$$\hat{L}^{Hb}_{h\xi}=\frac{1}{2\sqrt{2}}[c_\xi^+c_\epsilon+c_\epsilon^+c_\xi+\sqrt{3}(c_\xi^+c_\theta+c_\theta^+c_\xi)],$$

$$\hat{L}^{Hb}_{h\eta}=\frac{1}{2\sqrt{2}}[c_\eta^+c_\epsilon+c_\epsilon^+c_\eta-\sqrt{3}(c_\eta^+c_\theta+c_\theta^+c_\eta)],$$

$$\hat{L}^{Hb}_{h\zeta}=-\frac{1}{\sqrt{2}}(c_\zeta^+c_\epsilon+c_\epsilon^+c_\zeta).$$

APPENDIX B: STATIONARY COORDINATES AND R FUNCTIONS

1. Stationary coordinates

$$\langle Q_{h\theta}\rangle=\frac{1}{2\sqrt{6}K_h}\Big\{(1+2\epsilon^2-3\zeta^2-4\theta^2)F_{Ha}+[3(\eta^2-\xi^2)-2\sqrt{3}\epsilon\theta]F_{Hb}-3\sqrt{\frac{2}{5}}(\phi^{-1}x^2-\phi y^2+z^2)F_{T_1}\Big\},$$

$$\langle Q_{h\epsilon}\rangle=\frac{1}{2\sqrt{2}K_h}\Big\{(\eta^2-\xi^2+2\sqrt{3}\theta\epsilon)F_{Ha}+(2\epsilon^2+3\zeta^2-1)\times F_{Hb}-\sqrt{\frac{2}{5}}(\phi^2x^2-\phi^{-2}y^2-\sqrt{5}z^2)F_{T_1}\Big\},$$

$$\langle Q_{h\xi}\rangle=\frac{1}{\sqrt{6}K_h}\Big\{[2\sqrt{2}\eta\zeta+(\theta-\sqrt{3}\epsilon)\xi]F_{Ha}-\sqrt{3}(\epsilon+\sqrt{3}\theta)\xi F_{Hb}-\frac{6}{\sqrt{5}}yzF_{T_1}\Big\},$$

$$\langle Q_{h\eta}\rangle = \frac{1}{\sqrt{6}K_h}\left\{[2\sqrt{2}\xi\zeta + (\theta+\sqrt{3}\epsilon)\eta]F_{Ha} - \sqrt{3}(\epsilon-\sqrt{3}\theta)\eta F_{Hb} - \frac{6}{\sqrt{5}}zxF_{T_1}\right\},$$

$$\langle Q_{h\zeta}\rangle = \frac{1}{\sqrt{3}K_h}\left\{(2\eta\xi - \sqrt{2}\theta\zeta)F_{Ha} + \sqrt{6}\epsilon\zeta F_{Hb} - 3\sqrt{\frac{2}{5}}xyF_{T_1}\right\},$$

where $\phi = \frac{1}{2}(1+\sqrt{5})$ is the golden mean.

2. *R* functions

$$R_A^{T_1} = \frac{1}{\sqrt{3}}(x^2+y^2+z^2) = \frac{1}{\sqrt{3}},$$

$$R_{H\theta}^{T_1} = \frac{1}{2}(\phi^{-1}x^2 - \phi y^2 + z^2),$$

$$R_{H\epsilon}^{T_1} = \frac{1}{2\sqrt{3}}(\phi^2x^2 - \phi^{-2}y^2 - \sqrt{5}z^2),$$

$$R_{H\xi}^{T_1} = \sqrt{2}yz,$$

$$R_{H\eta}^{T_1} = \sqrt{2}zx,$$

$$R_{H\zeta}^{T_1} = \sqrt{2}xy,$$

$$R_A^H = \frac{1}{\sqrt{5}}(\theta^2+\epsilon^2+\xi^2+\eta^2+\zeta^2) = \frac{1}{\sqrt{5}},$$

$$R_{Ga}^H = \sqrt{\frac{3}{10}}(\theta^2+\epsilon^2) - \sqrt{\frac{2}{15}}(\xi^2+\eta^2+\zeta^2),$$

$$R_{Gx}^H = -\frac{1}{\sqrt{3}}(\theta-\sqrt{3}\epsilon)\xi + \frac{2}{\sqrt{6}}\eta\zeta,$$

$$R_{Gy}^H = -\frac{1}{\sqrt{3}}(\theta+\sqrt{3}\epsilon)\eta + \frac{2}{\sqrt{6}}\xi\zeta,$$

$$R_{Gz}^H = \frac{2}{\sqrt{3}}\theta\zeta + \frac{2}{\sqrt{6}}\xi\eta,$$

$$R_{H\theta}^{Ha} = \frac{1}{2}\sqrt{\frac{3}{2}}(\theta^2-\epsilon^2) - \frac{1}{2\sqrt{6}}(\xi^2+\eta^2-2\zeta^2),$$

$$R_{H\epsilon}^{Ha} = -\sqrt{\frac{3}{2}}\theta\epsilon + \frac{1}{2\sqrt{2}}(\xi^2-\eta^2),$$

$$R_{H\xi}^{Ha} = -\frac{1}{\sqrt{6}}(\theta-\sqrt{3}\epsilon)\xi - \frac{2}{\sqrt{3}}\eta\zeta,$$

$$R_{H\eta}^{Ha} = -\frac{1}{\sqrt{6}}(\theta+\sqrt{3}\epsilon)\eta - \frac{2}{\sqrt{3}}\xi\zeta,$$

$$R_{H\zeta}^{Ha} = \frac{2}{\sqrt{6}}\theta\zeta - \frac{2}{\sqrt{3}}\xi\eta,$$

$$R_{H\theta}^{Hb} = \frac{1}{\sqrt{2}}\theta\epsilon + \frac{1}{2}\sqrt{\frac{3}{2}}(\xi^2-\eta^2),$$

$$R_{H\epsilon}^{Hb} = \frac{1}{2\sqrt{2}}(\theta^2-\epsilon^2+\xi^2+\eta^2-2\zeta^2),$$

$$R_{H\xi}^{Hb} = \frac{1}{\sqrt{2}}(\sqrt{3}\theta+\epsilon)\xi,$$

$$R_{H\eta}^{Hb} = -\frac{1}{\sqrt{2}}(\sqrt{3}\theta-\epsilon)\eta,$$

$$R_{H\zeta}^{Hb} = -\sqrt{2}\epsilon\zeta.$$

APPENDIX C: ANGULAR MOMENTUM OPERATORS IN *Q* SPACE

$$\hat{L}_x(Q) = -\frac{\phi^2}{\sqrt{2}}(Q_1\hat{P}_3 - Q_3\hat{P}_1) + \sqrt{\frac{3}{2}}\phi^{-1}(Q_2\hat{P}_3 - Q_3\hat{P}_2) + (Q_5\hat{P}_4 - Q_4\hat{P}_5),$$

$$\hat{L}_y(Q) = \frac{\phi^{-2}}{\sqrt{2}}(Q_1\hat{P}_4 - Q_4\hat{P}_1) - \sqrt{\frac{3}{2}}\phi(Q_2\hat{P}_4 - Q_4\hat{P}_2) + (Q_3\hat{P}_5 - Q_5\hat{P}_3),$$

$$\hat{L}_z(Q) = \sqrt{\frac{5}{2}}(Q_1\hat{P}_5 - Q_5\hat{P}_1) + \sqrt{\frac{3}{2}}(Q_2\hat{P}_5 - Q_5\hat{P}_2) + (Q_4\hat{P}_3 - Q_3\hat{P}_4),$$

where

$$\hat{P}_k = -i\hbar\frac{\partial}{\partial Q_k}.$$

*Electronic address: Arnout.Ceulemans@chem.kuleuven.ac.be

[1] C.C. Chancey and M.C.M. O'Brien, *The Jahn-Teller Effect in* C_{60} *and Other Icosahedral Complexes* (Princeton University Press, New Jersey, 1997).

[2] D.J. van den Heuvel, G.J.B. van den Berg, E.J.J. Groenen, J. Schmidt, I. Holleman, and G. Meijer, J. Phys. Chem. **99**, 11 644 (1995).

[3] A. Sassara, G. Zerza, and M. Chergui, J. Phys. B **29**, 4997 (1996).

[4] F. Negri, G. Orlandi, and F. Zerbetto, J. Chem. Phys. **97**, 6496 (1992).
[5] S. Suzuki, D. Inomata, N. Sashide, and K. Nakao, Phys. Rev. B **48**, 14 615 (1993).
[6] F. Negri and G. Orlandi, in *Proceedings of XIV International Symposium on Electron-Phonon Dynamics and Jahn-Teller Effect, Erice, Italy, 1998*, edited by G. Bevilacqua, L. Martinelli, and N. Terzi (World Scientific, Singapore, 1999), p. 264.
[7] A. Ceulemans and Q.C. Qiu, Phys. Rev. B **61**, 10 628 (2000).
[8] R.D. Bendale, J.D. Baker, and M.C. Zerner, Int. J. Quantum Chem., Symp. **25**, 557 (1991).
[9] P.W. Fowler and A. Ceulemans, Mol. Phys. **54**, 767 (1985).
[10] L.L. Boyle and Y.M. Parker, Mol. Phys. **39**, 95 (1980).
[11] A. Ceulemans, J. Chem. Phys. **87**, 5374 (1987).
[12] A. Ceulemans and L.F. Chibotaru, Theor. Chim. Acta **94**, 205 (1996).
[13] U. Oepik and M.H.L. Pryce, Proc. R. Soc. London, Ser. A **238**, 425 (1957).
[14] A. Ceulemans and L.G. Vanquickenborne, Struct. Bonding (Berlin) **71**, 125 (1989).
[15] J.L. Dunn and C.A. Bates, Phys. Rev. B **52**, 5996 (1995).
[16] Q.C. Qiu, J.L. Dunn, C.A. Bates, and Y.M. Liu, Phys. Rev. B **58**, 4406 (1998).
[17] Q.C. Qiu, J.L. Dunn, C.A. Bates, M. Abou-Ghantous, and V.Z. Polinger, Phys. Rev. B **62**, 16 155 (2000).
[18] A. Ceulemans and P.W. Fowler, J. Chem. Phys. **93**, 1221 (1990).
[19] D.R. Pooler, J. Phys. C **13**, 1029 (1980).
[20] B.R. Judd and E. Lo, J. Phys. B **32**, 1073 (1999).
[21] A. Ceulemans, G. Mys, and Z. Walcerz, New J. Chem. **17**, 131 (1993).
[22] V.P. Khlopin, V.Z. Polinger, and I.B. Bersuker, Theor. Chim. Acta **48**, 87 (1978).
[23] N. Manini and P. De Los Rios, J. Phys.: Condens. Matter **10**, 8485 (1998).
[24] A. Sassara, G. Zerza, M. Chergui, F. Negri, and G. Orlandi, J. Chem. Phys. **107**, 8731 (1997).
[25] I. B. Bersuker and V. Z. Polinger, *Vibronic Interactions in Molecules and Crystals* (Springer, Berlin, 1989).